Phys. Status Solidi RRL **4**, No. 10, 265–267 (2010) / **DOI** 10.1002/pssr.201004049

pss +++rapid research letters+++
www.pss-rapid.com

Multiple surface-plasmon-polariton waves localized to a metallic defect layer in a sculptured nematic thin film

Muhammad Faryad and Akhlesh Lakhtakia*

Nanoengineered Metamaterials Group, Department of Engineering Science and Mechanics, Pennsylvania State University, University Park, PA 16802, USA

Received 19 February 2010, revised 17 March 2010, accepted 18 March 2010
Published online 22 March 2010

Keywords plasmons, polaritons, wave optics, optical materials

* Corresponding author: e-mail akhlesh@psu.edu, Phone: +1-814-863-4319, Fax: +1-814-865-9974

The propagation of a surface-plasmon-polariton (SPP) wave guided by a thin metallic defect layer in a sculptured nematic thin film (SNTF) – a periodically nonhomogeneous, anisotropic, dielectric material – was studied theoretically. If the defect layer is sufficiently thick, SPP waves propagate independently along the two metal/SNTF interfaces formed by the presence of the defect layer in the SNTF. As the thickness of the defect layer is reduced, SPP wave propagation is modified by the coupling of the two interfaces. The number of SPP waves increases and lower attenuation rates along the direction of propagation become possible.

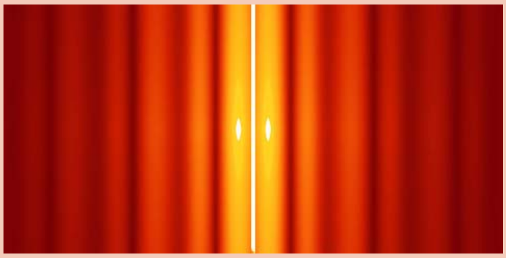

1 Introduction Surface-plasmon-polariton (SPP) waves propagate localized to the planar interface of a metal and a dielectric material [1, 2]. SPP wave propagation is under intense scrutiny currently due to a wide variety of applications in sensing, communication and microscopy [3]. If the partnering dielectric material is homogeneous and isotropic, only one SPP wave at a specific frequency can be excited along the interface. Periodic nonhomogeneity of the dielectric partnering material normal to the interface appears necessary for the ability to excite multiple SPP waves – of different phase speeds, attenuation rates, and field structures – at a specific frequency. The periodically nonhomogeneous material can be isotropic [4] or anisotropic, with the latter providing more options [5, 6].

In a bid to further increase the number of SPP waves excitable at a specific frequency, we decided to theoretically investigate wave propagation localized to a metallic defect layer in a sculptured nematic thin film (SNTF) – a periodically nonhomogeneous and anisotropic dielectric material grown by physical vapor deposition [4]. The possibility of multiple SPP waves localized to the interface of a metal and an SNTF has been demonstrated both theoretically [5, 7] and experimentally [8]. A metallic defect layer provides two metal/dielectric interfaces, the coupling of which could increase the number of SPP waves. This possibility has been known for long when the dielectric materials are isotropic [9, 10], but our focus here is on the anisotropic SNTFs.

This letter contains our preliminary but encouraging results. Section 2 contains the guidelines to synthesize the theory, whereas numerical results are presented in Section 3. An $\exp(-i\omega t)$ time dependence is implicit, with ω denoting the angular frequency. The free-space wavenumber and the free-space wavelength are denoted by $k_0 = \omega\sqrt{\varepsilon_0\mu_0}$ and $\lambda_0 = 2\pi/k_0$, respectively, with μ_0 and ε_0 being the permeability and permittivity of free space. Vectors are in boldface and dyadics are underlined twice. The Cartesian unit vectors are identified as $\hat{\boldsymbol{u}}_x$, $\hat{\boldsymbol{u}}_y$, and $\hat{\boldsymbol{u}}_z$.

2 Theory Let the region $L_- \le z \le L_+$ be occupied by an isotropic and homogeneous metal with complex-valued relative permittivity scalar $\varepsilon_{\rm met}$. The regions $z > L_+$ and $z < L_-$ are occupied by the chosen SNTF. An SNTF is an array of parallel nanocolumns whose shape is engineered by appropriately directing the vapor flux during fabrication. Therefore, the permittivity dyadic of a periodically nonhomogeneous SNTF may be stated as [5, 7, 8]

$$\underline{\underline{\varepsilon}}_{\rm SNTF}(z) = \varepsilon_0 \underline{\underline{S}}_z(\gamma)\cdot\underline{\underline{S}}_y(z)\cdot\underline{\underline{\varepsilon}}^{\circ}_{\rm ref}(z)\cdot\underline{\underline{S}}_y^{-1}(z)\cdot\underline{\underline{S}}_z^{-1}(\gamma)\,,\quad z \gtrless L_\pm \tag{1}$$

wherein the locally orthorhombic symmetry is expressed through the diagonal dyadic

$$\underline{\underline{\varepsilon}}^{\circ}_{\rm ref}(z) = \varepsilon_a(z)\,\hat{\boldsymbol{u}}_z\hat{\boldsymbol{u}}_z + \varepsilon_b(z)\hat{\boldsymbol{u}}_x\hat{\boldsymbol{u}}_x + \varepsilon_c(z)\hat{\boldsymbol{u}}_y\hat{\boldsymbol{u}}_y\,, \tag{2}$$

and the nanocolumnar morphology by the tilt dyadic

$$\underline{\underline{S}}_y(z) = (\hat{\boldsymbol{u}}_x\hat{\boldsymbol{u}}_x + \hat{\boldsymbol{u}}_z\hat{\boldsymbol{u}}_z)\cos[\chi(z)] + (\hat{\boldsymbol{u}}_z\hat{\boldsymbol{u}}_x - \hat{\boldsymbol{u}}_x\hat{\boldsymbol{u}}_z)\sin[\chi(z)] + \hat{\boldsymbol{u}}_y\hat{\boldsymbol{u}}_y\,. \tag{3}$$

The relative permittivity scalars $\varepsilon_{a,b,c}(z)$ and the tilt angle $\chi(z)$ depend on the vapor incidence angle

$$\chi_v(z) = \tilde{\chi}_v \pm \delta_v \sin\left[\frac{\pi(z-L_\pm)}{\Omega}\right],\quad z \gtrless L_\pm\,, \tag{4}$$

that varies sinusoidally with z, the chosen dependences being described in Section 3. The third dyadic on the right side of Eq. (1),

$$\underline{\underline{S}}_z(\gamma) = (\hat{\boldsymbol{u}}_x\hat{\boldsymbol{u}}_x + \hat{\boldsymbol{u}}_y\hat{\boldsymbol{u}}_y)\cos\gamma + (\hat{\boldsymbol{u}}_y\hat{\boldsymbol{u}}_x - \hat{\boldsymbol{u}}_x\hat{\boldsymbol{u}}_y)\sin\gamma + \hat{\boldsymbol{u}}_z\hat{\boldsymbol{u}}_z\,, \tag{5}$$

indicates that the plane formed by the unit vectors $\hat{\boldsymbol{u}}_z$ and $\hat{\boldsymbol{u}}_x\cos\gamma + \hat{\boldsymbol{u}}_y\sin\gamma$ is the morphologically significant plane of the SNTF [5].

Without loss of generality, let us choose the direction of SPP wave propagation in the x,y-plane to be parallel to the x axis. Accordingly, we set

$$\boldsymbol{E}(\boldsymbol{r}) = \boldsymbol{e}(z)\exp(i\kappa x)\,,\quad \boldsymbol{H}(\boldsymbol{r}) = \boldsymbol{h}(z)\exp(i\kappa x)\,, \tag{6}$$

where κ is a complex-valued scalar. To find the values of complex κ, the procedure described by Faryad et al. [7] was adapted as follows: Eq. (6) was substituted in the Maxwell curl equations and a matrix ordinary differential equation (MODE) was obtained for each region: $z < L_-$, $L_- < z < L_+$, and $z > L_+$. The standard boundary conditions were enforced across the interfaces $z = L_\pm$, and the condition that the fields must decay as $z \to \pm\infty$ were imposed on the solutions of the MODEs to obtain the dispersion equation for the SPP waves localized to the metallic defect layer.

3 Results and discussion A Mathematica™ program was written and implemented to solve the dispersion equation to obtain κ for a specific value of γ. The free-space wavelength was fixed at $\lambda_0 = 633$ nm. The metal was taken to be aluminum: $\varepsilon_{\rm met} = -56 + 21i$. The SNTF was chosen to be made of titanium oxide [5, 7], with

$$\left.\begin{aligned} \varepsilon_a(z) &= [1.0443 + 2.7394v(z) - 1.3697v^2(z)]^2 \\ \varepsilon_b(z) &= [1.6765 + 1.5649v(z) - 0.7825v^2(z)]^2 \\ \varepsilon_c(z) &= [1.3586 + 2.1109v(z) - 1.0554v^2(z)]^2 \\ \chi(z) &= \tan^{-1}[2.8818\tan\chi_v(z)] \end{aligned}\right\}, \tag{7}$$

where $v(z) = 2\chi_v(z)/\pi$. The angles $\tilde{\chi}_v$ and δ_v were taken to be 45° and 30°, respectively, for all results presented here. The dispersion equation for SPP wave propagation was solved for $L_\pm = \pm 45$, ± 25, ± 12.5, and 7.5 nm Solutions were searched for $\mathrm{Re}\,(\kappa/k_0) \in [1.5, 3.0]$.

For the thickest metallic defect layer, we found that, as functions of γ, the values of κ that satisfy the dispersion equation for SPP wave propagation localized to the metallic defect layer are organized in three branches, as shown in Fig. 1. There are three values of κ for a specific $\gamma \in [0°, 36°]$, but only two for a specific $\gamma \in (36°, 90°]$. Recalling that γ is the angle between the direction of propagation (x-axis) and the morphologically significant plane of the SNTF, we see that the data in Fig. 1 are exactly the same as those for a single metal/SNTF interface [7]. Since the penetration depth – defined as the distance from the interface along the z-axis at which the field decays to $1/e$ of its value at the interface – for SPP waves guided by a single metal/SNTF interface is on the order of 12.7 nm in the metal [7], and the metallic defect layer is 90 nm thick, the two interfaces $z = L_\pm$ of the metallic defect layer with the SNTF are separately guiding SPP waves. In other words, SPP waves guided by the interface $z = L_+$ are not coupled to the SPP waves guided by the interface $z = L_-$, but have the same phase speed and attenuation rate along the direction of propagation.

Reducing the thickness of the defect layer to 50 nm, we found that the $\kappa - \gamma$ relationship is organized in five branches, as shown in Fig. 2. The two branches spanning the full range of γ in in Fig. 1 split into two branches each in Fig. 2, wherein five values of κ satisfy the dispersion equation for $\gamma \in [0°, 35°]$, four for $\gamma \in (35°, 37°]$, and three for $\gamma \in (37°, 90°]$. The splitting of branches relative to those in the figure for the thicker defect layer indicates that there is now some coupling between the the two metal/SNTF interfaces.

The coupling intensifies as the thickness of the metallic defect layer is reduced further to 25 nm, which is about twice the penetration depth (~12.7 nm) in metal for SPP wave propagation guided by a single metal/SNTF interface alone. The number of solution branches remains five in Fig. 3: five values of κ satisfy the dispersion equation for $\gamma \in [0°, 49°]$ and four for $\gamma \in (49°, 90°]$. Finally, when the metal defect layer is very thin (15 nm), Fig. 4 shows that there are still five solution branches, but now all five span the complete range $0° \le \gamma \le 90°$. This case shows very strong coupling between the two interfaces $z = L_\pm$.

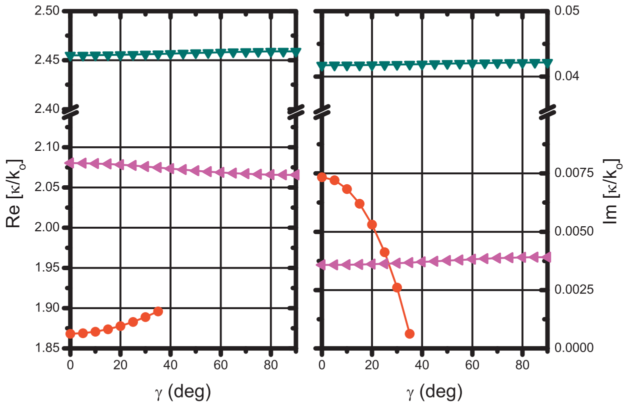

Figure 1 (online colour at: www.pss-rapid.com) (left) Real and (right) imaginary parts of κ as functions of γ for $L_\pm = \pm 45$ nm.

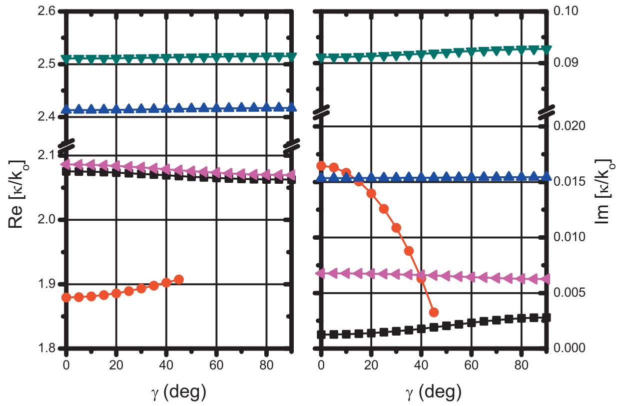

Figure 3 (online colour at: www.pss-rapid.com) Same as Fig. 1 except for $L_\pm = \pm 12.5$ nm.

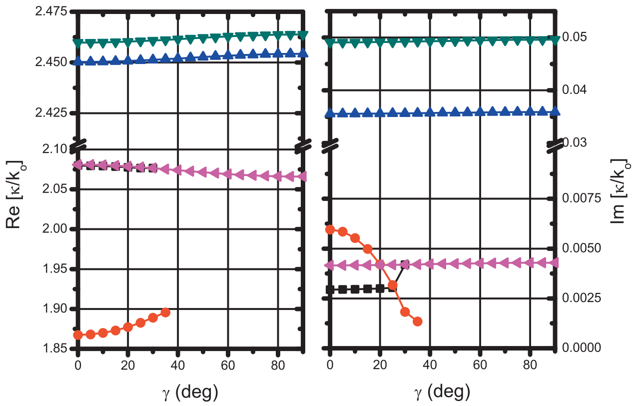

Figure 2 (online colour at: www.pss-rapid.com) Same as Fig. 1 except for $L_\pm = \pm 25$ nm.

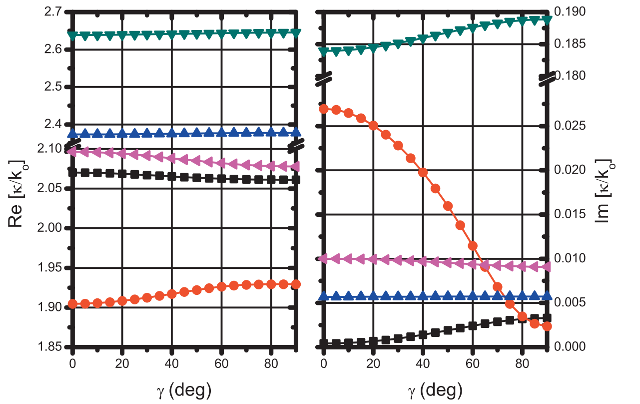

Figure 4 (online colour at: www.pss-rapid.com) Same as Fig. 1 except for $L_\pm = \pm 7.5$ nm.

Comparison of Figs. 1–4 shows that the SPP waves with higher e-folding distance $1/\mathrm{Im}(\kappa)$ of the field along the direction of propagation can exist over a greater range of γ as the defect thickness becomes smaller. For instance, the e-folding distance is greater than 40 µm only for $\gamma \in [30°, 36°]$ with the 90 nm thick defect layer, but that γ-range expands to $0° \le \gamma \le 60°$ for the 15 nm thick defect layer.

4 Concluding remarks Theoretical investigation of SPP wave propagation localized to a metallic defect layer in a periodically nonhomogeneous sculptured nematic thin film has shown that, if the defect layer is sufficiently thick, each of the two metal/SNTF interfaces guides SPP waves all by itself. If the defect layer is sufficiently thin, however, the two interfaces couple to each other, thereby enabling the emergence of new SPP waves. The attenuation rates along the direction of propagation are also lowered. The latter characteristic would be helpful for long-range communication while the former could be useful for multi-channel communication.

Acknowledgement MF thanks the Trustees of the Pennsylvania State University for a University Graduate Fellowship.

References

[1] S. A. Maier, Plasmonics: Fundamentals and Applications (Springer, New York, 2007).
[2] J. A. Polo, Jr. and A. Lakhtakia, Laser & Photon. Rev., **DOI:** 10.1002/lpor.200900050 (2010).
[3] J. Homola (ed.), Surface Plasmon Resonance Based Sensors (Springer, Heidelberg, 2006).
[4] Y.-J. Jen, A. Lakhtakia, C.-W. Yu, and T.-Y. Chan, J. Opt. Soc. Am. A **26**, 2600–2606 (2009).
[5] M. A. Motyka and A. Lakhtakia, J. Nanophoton. **3**, 033502 (2009).
[6] J. A. Polo, Jr. and A. Lakhtakia, Proc. R. Soc. Lond. A **465**, 87–107 (2009).
[7] M. Faryad, J. A. Polo, Jr., and A. Lakhtakia, J. Nanophoton. **4**, 043505 (2010).
[8] A. Lakhtakia, Y.-J. Jen, and C.-F. Lin, J. Nanophoton. **3**, 033506 (2009).
[9] L. Wendler and R. Haupt, Phys. Status Solidi B **143**, 131–148 (1987).
[10] F. Yang, J. R. Sambles, and G. W. Bradberry, Phys. Rev. B **44**, 5855–5872 (1991).